# Effect of Photogenerated Carrier Distribution on Performance Enhancement of Photomultiplication organic photodetectors

WenyanWang[a] LinlinShi[a] YeZhang[a] GuohuiLi[a] YuyingHao[ab] FurongZhu[c] KaiyingWang[ad] YanxiaCui[ab]

[a]College of Physics and Optoelectronics, Taiyuan University of Technology, Taiyuan, 030024, China
[b] Key Laboratory of Interface Science and Engineering in Advanced Materials, Taiyuan University of Technology, Taiyuan, 030024, China
[c]Department of Physics, Institute of Advanced Materials, And Institute of Research and Continuing Education (Shenzhen), Hong Kong Baptist University, Kowloon Tong, Hong Kong, China
[d]Department of Microsystems, University of South-Eastern Norway, Horten, 3184, Norway

*Organic electronics, 68*, 56-62.
10.1016/j.orgel.2019.01.055

# Effect of Photogenerated Carrier Distribution on Performance Enhancement of Photomultiplication Organic Photodetectors

Wenyan Wang,[a] Linlin Shi,[a] Ye Zhang,[a] Guohui Li,[a] Yuying Hao,[a,b] Furong Zhu,[c] Kaiying Wang,[a, d] and Yanxia Cui[a,b,*]

[a]*College of Physics and Optoelectronics, Taiyuan University of Technology, Taiyuan 030024, China*

[b]*Key Laboratory of Interface Science and Engineering in Advanced Materials, Taiyuan University of Technology, Taiyuan 030024, China*

[c]*Department of Physics, Institute of Advanced Materials, and Institute of Research and Continuing Education (Shenzhen), Hong Kong Baptist University, Kowloon Tong, Hong Kong, China*

[d] *Department of Microsystems, University of Southeast Norway, Horten, 3184, Norway*

*Corresponding author*:* yanxiacui@gmail.com (Y. Cui)

ABSTRACT

The trap-assisted photomultiplication (PM) organic photodetectors (OPDs) are very attractive for achieving high sensitivity photodetection, with external quantum efficiency (EQE) in excess of 100%. A classic structure of PM-type OPDs has a poly-3-hexylthiophene (P3HT): Phenyl-$C_{70}$-butyric acid methyl ester ($PC_{70}BM$) blend active layer, made with the weight ratio of P3HT to $PC_{70}BM$ of 100:1. The presence of a low $PC_{70}BM$ content in the P3HT:$PC_{70}BM$ blend layer forms isolated $PC_{70}BM$

domains serving as the defect sites to trap the photogenerated electrons. The trapped electrons induce a strong interfacial band bending at the organic/metal contact (Al) interface assisting in an enhanced hole injection via tunneling effect. In this work, we report a comprehensive study to understand the effect of the distribution of the photogenerated charge carriers on performance of the PM OPDs, made of a P3HT:$PC_{70}BM$ active layer with different layer thicknesses, for optimizing the PM effect. The synergistic effect of both exciton generation and exciton dissociation processes affects the distribution of the photogenerated charge carriers and hence the PM processes in the OPDs. The simulation of optical properties of the PM OPDs points out that a stronger exciton generation exists near the organic/Al interface in PM OPD with a thinner active layer. The photoluminescence and surface morphology measurements show that a 230 nm thick active layer with a smooth surface had the highest exciton dissociation rate. A champion EQE of 105569% and a photoresponsivity of 344

A/W were obtained for a PM OPD with a 205 nm thick active layer, which are about 330% higher than that of the OPD with a 325 nm thick active layer. Due to the tradeoff between EQE and dark current, the OPD with a thin active layer (205 nm) yields a maximum detectivity of $1.87\times10^{13}$ Jones at the short wavelength range while the OPD with a thick active layer (325 nm) has the highest detectivity of $2.32\times10^{13}$ Jones at the long wavelength range. Our work contributes to the development of high performance low-cost PM OPDs for detecting weak light signals.

*Keywords:*
Organic photodetectors; photomultiplication effect; EQE; electron trap

# 1. Introduction

Recently, organic photodetectors (OPDs) [1-3] [4] have received tremendous interests because of

their unique advantages of abundant material choices, light weight, good flexibility, and solution fabrication processes at low-cost. The high sensitivity OPDs with an external quantum efficiency (EQE) in excess of 100% can be realized through photomultiplication (PM) effect[5-12], for detecting the weak light for applications in optical sensor, health monitoring and near infrared (NIR) imaging and tele-communication [13-15]. The PM type OPDs take the advantage of trap-assisted carrier tunneling effect[8, 16-18] in the optoelectronic conversion process, including light absorption in active layer, carrier generation/capture by traps after light illumination, carrier transport toward the Schottky junction under applied bias, and carrier tunneling through the Schottky barrier.

PM type OPDs made with the small organic molecules were reported, but their fabrication required expensive thin film deposition systems[4, 19-21]. In comparison, the solution processable functional polymer-based heterojunctions are better candidates for developing low cost PM type OPDs[22-27]. Among the diverse heterojunction formulas, polymer:fullerene blends with a weight ratio of polymer to fullerene of much higher than 1:1 are quite intensively investigated[10, 28-30]. In these kind of devices, the fullerene derivative acceptor forms isolated domains in the blend layer, serving as the defect sites to trap the photogenerated charge carriers, and thereby inducing the current multiplication. Its pioneer prototype with a configuration of indium tin oxide (ITO)/poly-3,4- ethylenedioxythiophene/poly-styrenesulfonate (PEDOT:PSS)/poly-3-hexylthiophene (P3HT): phenyl-$C_{71}$-butyric acid methyl ester ($PC_{71}BM$)(100:1)/LiF/Al was demonstrated in 2015[31], with an EQE of 16700% at -19 V bias. A much higher EQE of 37500% was demonstrated by lowering the hole injection barrier at the organic/Al interface through the removal of the LiF buffer layer

[8]. Furthermore, an EQE of 115800% was achieved by controlling the face-on arranged P3HT molecules in the P3HT:$PC_{70}BM$ blend for facilitating the efficient hole transportation[24].

In this work, the performance of PM type OPDs was optimized through changing the thickness of the active layer. Our theoretical studies reflect that more excitons can be induced under light illumination near the Al electrode in a PM OPD with a thinner active layer. The experimental studies demonstrate that with the decrease of the thickness of the active layer from 325 nm to 205 nm thick, the EQE of the PM OPD are improved and further decrease of the active layer results in a reduction in EQE. The highest EQE of 105569% was realized at 405 nm wavelength under -17 V bias for the PM OPD with a 205 nm thick active layer, which is 330% higher as compared to that of the OPD with a 325 nm thick active layer. The following photoluminescence (PL) and surface morphology studies of films indicate that the active layer with different thicknesses possess different exciton dissociation rates and the 230 nm thick film has the optimal exciton dissociation rate. The combination of both the photogenerated exciton distribution and the exciton dissociation rate ultimately determines the photogenerated carrier distribution in the active layer, explaining why the OPD with the champion EQE has a 205 nm thick active layer. However, the decrease in the thickness of the active layer resulted in an increase in the dark current ($J_d$). Overall, the PM type OPDs with a 205 nm thick active layer possess the maximum detectivity ($D^*$) of $1.87\times10^{13}$ Jones at wavelength □ 500 nm, and the OPD with a 325 nm thick active layer had the maximum $D^*$ of $2.32\times10^{13}$ Jones at wavelength > 500 nm. Our work contributes to developing low cost and highly sensitive photodetectors.

## 2. Device structure and working mechanism

The schematic cross-sectional view of the PM OPD and the diagram of the energy levels of the materials used in the PM type OPDs, with a configuration of ITO (100 nm)/PEDOT:PSS (25

nm)/P3HT:$PC_{70}BM$/Al (100 nm), are shown in Figs. 1(a) and 1(b), respectively. The active layer is made of P3HT:$PC_{70}BM$ with the weight ratio of 100:1, in which the nano-sized islands of $PC_{70}BM$ molecules are dispersed in the P3HT matrix. In our study, the thickness of the active layer ($L$) varies from 180 nm to

325 nm. From Fig. 1(b), it is found that the difference in energy level between the lowest unoccupied molecular orbital (LUMO) levels of P3HT (-3.0 eV) and $PC_{70}BM$ (-4.3 eV) is 1.3 eV. With such a high energy barrier, the photogenerated electrons can be successfully trapped in the $PC_{70}BM$ islands. Moreover, the hole injection barrier is about 0.9 eV between the highest occupied molecular orbital (HOMO) levels of Al and P3HT, therefore the holes are hardly injected from the Fermi level of Al (−4.2 eV) cathode into the HOMO level of P3HT (−5.1 eV). However, under illumination, holes might tunnel from the Al electrode to P3HT due to the existence of electron traps in the active layer. When a bias is applied with the electric field pointing from Al to ITO, the photogenerated electrons trapped by the $PC_{70}BM$ islands are able to transport toward the P3HT:$PC_{70}BM$/Al junction, resulting in a large amount of electrons aggregate near the Al electrode. The aggregation of electrons will induce interfacial band bending and a corresponding narrower barrier, which finally results in stronger hole tunneling into the P3HT HOMO

level, i.e., a higher current multiplication factor.

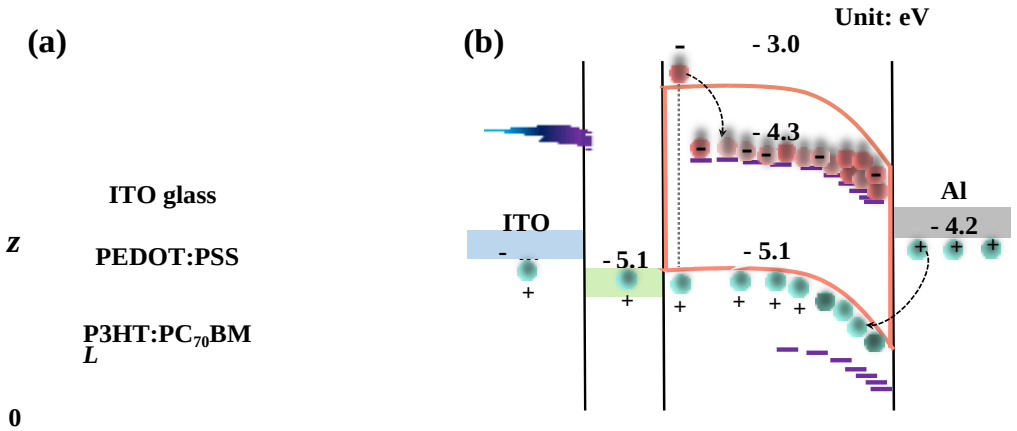

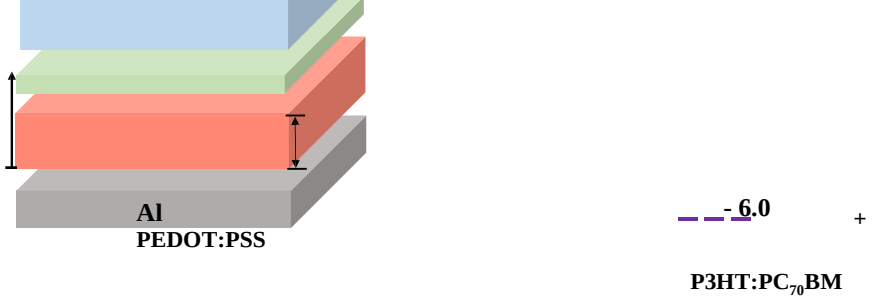


Fig. 1. (a) The schematic cross-sectional view of the PM type OPD, and (b) the diagram of the energy levels of the materials used in the PM OPD.

## 3. Simulation section

### 3.1 *Simulation methods*

The optical properties of the PM type OPDs are investigated theoretically by the two-dimensional (2D) Finite Element Method (FEM) [32, 33]. All simulations were carried out assuming a periodic boundary along the *z* axis, which is normal to the film plane. Perfectly matched layer (PML) boundaries are applied at two planes perpendicular to the *z* axis, one lies in the glass and the other is in the air region next to the Al electrode. Light is illuminated from the ITO glass side. The wavelength dependent refractive indices and extinction coefficients of the P3HT:$PC_{70}BM$ (100:1) layer are obtained from Ref. [29]. The refractive indices and extinction coefficients of other materials used in this work are extracted from Refs. [34, 35]. The exciton generation originates from the absorption of photons, so we calculated the wavelength-dependent absorption efficiency, $\eta(\lambda)$, of the active layer, and the corresponding integrated absorption efficiency ($\eta_I$) over the wavelength range between 300 nm and 650 nm was also calculated.

### 3.2 *Simulation results and discussion*

Figs. 2(a) and 2(b) show the curves of $\eta(\lambda) \sim \lambda$ at varied $L$ and the curve of $\eta_I \sim L$, respectively. It is seen clearly in Fig. 2(b) that when $L$ increases from 180 nm to 290 nm, $\eta_I$ increases gradually and further increase of $L$ leads to the reduction of $\eta_I$. Such tendency is because the absorption peak at the wavelength range shorter than 450 nm redshift with gradually enhanced intensity with the increase of $L$ as shown in Fig. 2(a). The local maxima of $\eta_I$ at $L$ = 290 nm reflects a very large amount of the incident light is absorbed in the active material. But such thick active layer may not be favorable in the

application of PM type OPDs because the photogenerated electrons in the region far away from the Al electrode could hardly arrive at the Al electrode due to poor electron transport property of the

P3HT:$PC_{70}BM$(100:1) layer, thereby contributing negligibly to strengthen the hole tunneling from the external circuit. Therefore, it is necessary to further examine the absorption maps.

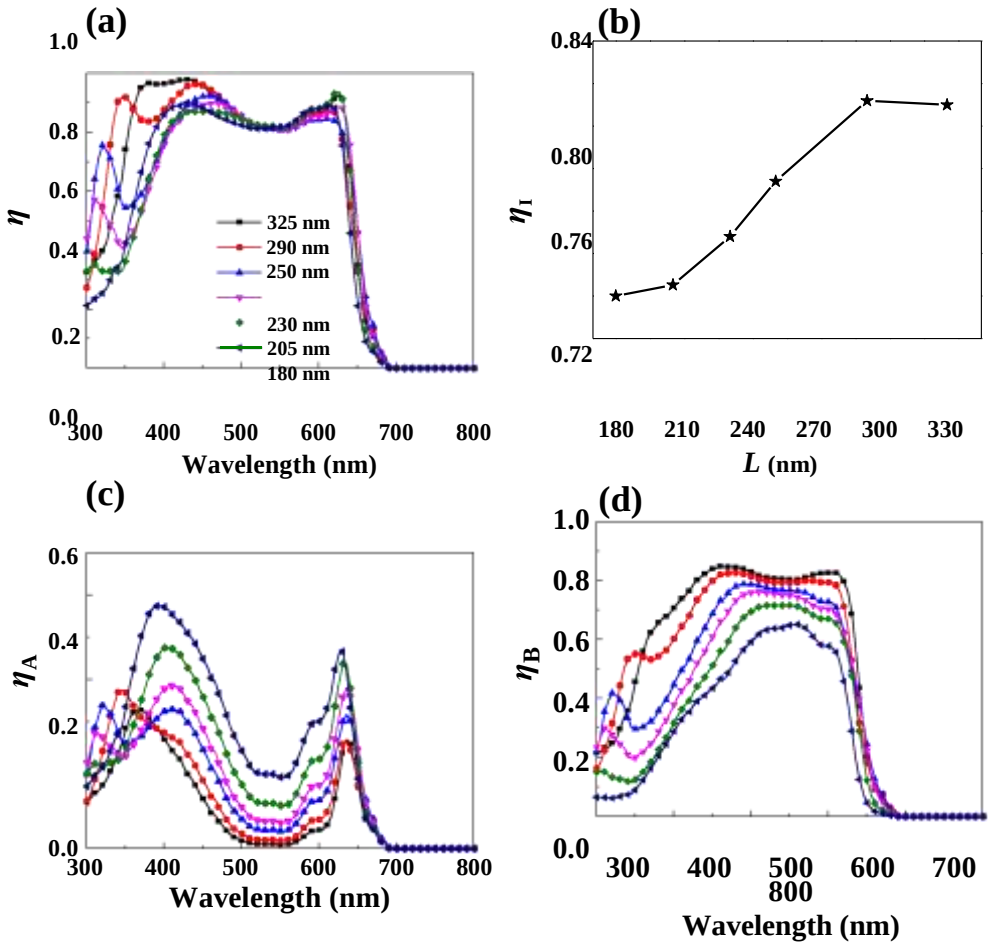


Fig. 2. (a) The wavelength-dependent absorption efficiency □(□) of the whole active layer over the wavelength range from 300 nm to 800 nm, and (b) the corresponding integrated absorption efficiency ($\eta_I$), calculated over the wavelength range from 300 nm to 650 nm, as a function of the active layer thickness ($L$). (c) The wavelength-dependent absorption efficiency in part A $\eta_A$( □)and (d) part B $\eta_B$( □)of the OPDs as a function of $L$. Part A is the region within 100 nm from the Al electrode, and Part B is the remaining region as indicated in Fig. 3.

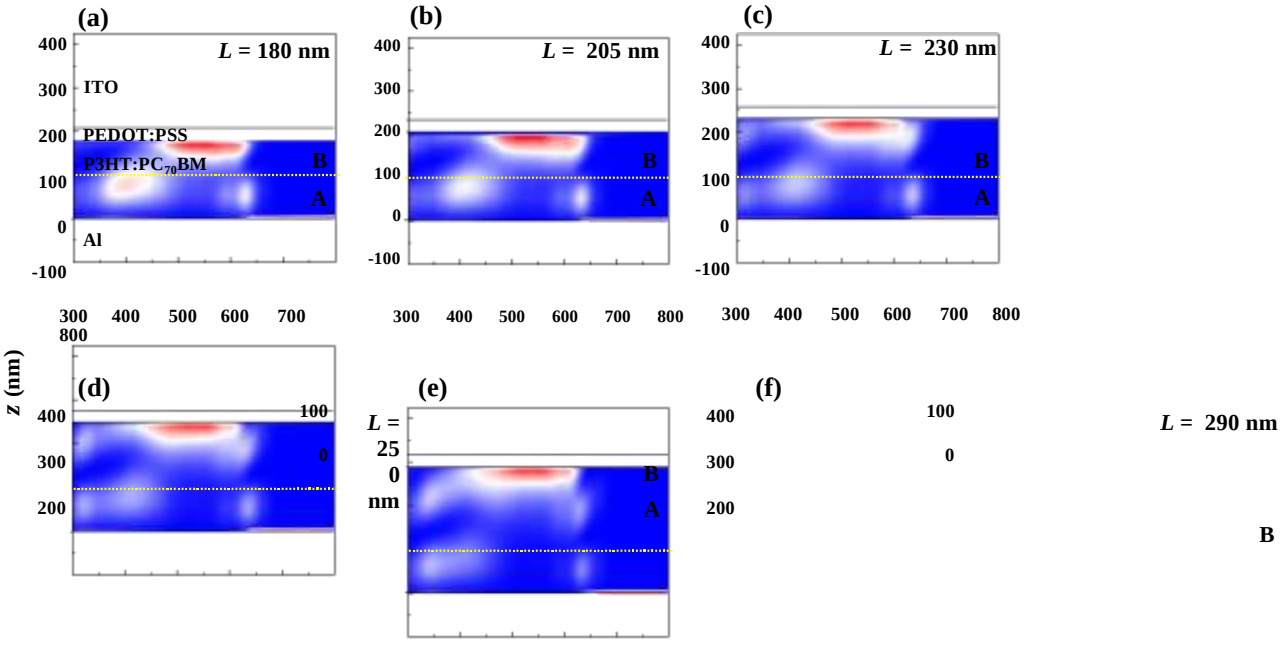

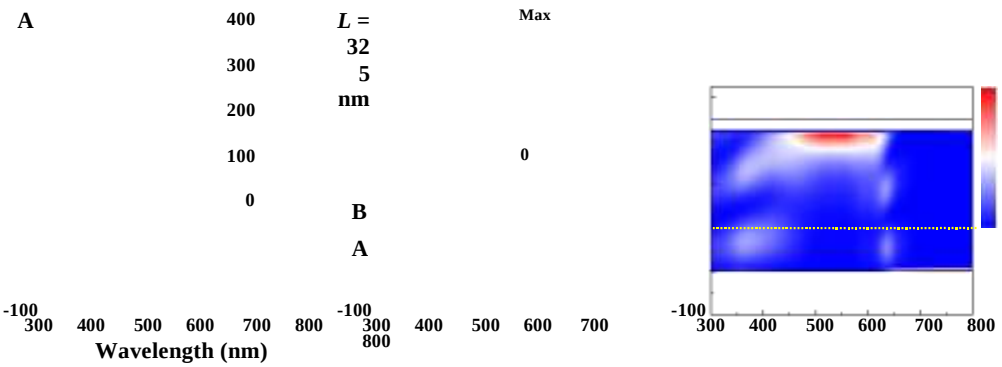
A
400
300
200
100
0
L = 325 nm
Max
0
B
A
-100
300 400 500 600 700 800
-100
300 400 500 600 700 800
Wavelength (nm)
-100
300 400 500 600 700 800

Fig. 3. Wavelength dependent maps of absorption in OPDs with different active layer thicknesses of (a) 180 nm, (b) 205 nm, (c) 230 nm, (d) 250 nm, (e) 290 nm, and (f) 325 nm.

Fig. 3 shows the maps of the wavelength dependent absorption distributions of the active layer with thickness from 180 nm to 325 nm. Those maps exhibit several bright spots due to the Fabry-Pérot interference effect [36], which correspond to efficient absorption by the active material. The most bright interference spots centered at wavelength of ~ 525 nm locate near the PEDOT:PSS layer, and its distance from the Al electrode becomes smaller when the active layer is thinner. In addition, although the active layer with $L$ = 290 nm allows more interference bright spots spread out inside it at wavelengths shorter than 450 nm and longer than 600 nm, the intensities of its interference spots close to the Al electrode are much weaker, with respect to the thin active layer cases (e.g., $L$ = 180 nm or 205 nm). To quantify the absorption intensity near the Al electrode, we then divided the active layer into two parts. The region within 100 nm from the Al electrode is labelled as Part A and the remaining region is Part B as shown in Fig. 3. Then, the absorption of light in Part A $\eta_A(\lambda)$ and Part B $\eta_B(\lambda)$ versus wavelength are calculated, respectively, at varied $L$, as displayed in Figs. 2(c) and 2(d). Obviously, it can be seen, although the absorption in the whole active layer is weakened in thin active layers, the absorption in Part A increases gradually with the decrease of the thickness of the active layer. Instead, the absorption in Part B in the active layer decreases gradually when the active layer becomes thicker. From the simulation results, we conclude that the thickness of the active layer determines the distribution of the absorption in the active layer and therefore the exciton generation distributions, playing a great influence on the performances of OPDs.

## 4. Experiment section

### 4.1 *Experiment details*

The ITO-coated glass substrates with a sheet resistance of 15 Ω/square were cleaned sequentially by

ultrasonication in detergent, deionized water, and ethanol each for 15 min. The wet-cleaned ITO/glass substrates were then dried by air and subjected to the surface plasma treatment for 5 min prior to the OPD fabrication, for increasing the work function of ITO substrates. The solution of PEDOT:PSS (purchased from Xi'an p-OLED) was coated on the cleaned ITO/glass substrates by spin-coating at 5000 rotations per minute (rpm) for 30 s, following with an annealing in air at 120 °C for 15 min. P3HT (from Xi'an p-OLED) and $PC_{70}BM$ (from 1-Material Corporation) were dissolved in 1,2-dichlorobenzene (o-DCB) to prepare 40 mg/ml mixed solution at the weight ratio of 100:1. The mixed solution was spin-coated on the PEDOT:PSS films at a certain spin speed for 30 s in nitrogen-purged glove box, then the samples were annealed at 80 °C for 20 s. The active layers with different layer thicknesses of 325 nm, 290 nm, 250 nm, 230 nm, 205 nm, and 180 nm, were prepared using spin speeds of 800 rpm, 1000 rpm, 1200 rpm, 1400 rpm, 1600 rpm, and 1800 rpm, respectively. The relationship between the spin speed and the thickness of the active layer is almost linear. Then, the 100 nm thick aluminum electrode was deposited on the active layer by thermal evaporation in a vacuum chamber with a base pressure of $10^{-4}$ Pa. The active area of the PM OPDs was about 0.04 $cm^2$, defined by the overlap of Al cathode and ITO anode.

The thicknesses of the spin-coated and evaporated films were characterized by profiler (Bruker, DektakXT). The current density–voltage (*J*–*V*) characteristics of OPDs in the dark and under illumination (with a burn-in treatment [9]) were measured using a programmable source meter (Keithley 2400). The monochromatic light source was supplied by a xenon lamp (ZOLIX GLORIA-X150A) combined with a monochromator (ZOLIX 0mni-$\lambda$ 3005) with the light intensities at varied wavelengths characterized by a power meter (Ophir NOVA II). The surface morphology of the P3HT:$PC_{70}BM$ active layer was characterized by the atomic force microscope (AFM) (Flying Man,

Nanoview 1000). The absorption spectra of multilayer films were measured using a Hitachi U-3900. The steady state photoluminescence (PL) spectra of films were measured using a fluorescence spectrophotometer (Edinburgh Instruments, FLS-980).

4.2 *Definition of performance parameters*

The performance parameters of the OPDs including EQE, photoresponsivity, detectivity, and response time are defined as follows.

The EQE, defined as the electron number detected per incident photon, was calculated using the following equation:

$$\mathrm{EQE} = \frac{N_e}{N_p} = \frac{I_{ph}/e}{P_{in}/h\nu}, \quad (1)$$

where $N_e$ and $N_p$ are the numbers of detected electrons and incident photons, respectively, $I_{ph}$ is the photocurrent, $P_{in}$ is the intensity of the incident light, $h$ is the Planck's constant, $\nu$ is the frequency of light, and $e$ is the electron charge.

In the investigated PM type OPDs, the presence of deep electron traps by the $PC_{70}BM$ islands causes a long electron recombination lifetime, resulting in a high photocurrent amplification gain, similar to that happens in photoconductor type photodetectors. In photodetectors with gain mechanisms, EQE is equal to the gain in number. Based on the definition of gain, EQE can also be given by Equation (2):

$$\mathrm{EQE} = \frac{\tau}{T}, \quad (2)$$

where $\chi$ is the fraction of trapped electrons over the total amount of the photogenerated electrons, $\tau$ is the lifetime of trapped electrons, and $T$ is the transport time of the hole transporting across the active layer.

The photoresponsivity ($R$), defined as the ratio of photocurrent to the power intensity of incident light, can be expressed by Equation (3):

$$R = \frac{I_{ph}}{P_{in}} = \frac{I_l - I_d}{P_{in}}, \tag{3}$$

where $I_l$ is the current under light illumination, and $I_d$ is the dark current.

The detectivity ($D^*$) is the figure of merit for quantifying the capability of weak light detection, which can be derived from the photoresponsivity and the noise density. Considering that the noise current under dark is dominated by shot noise, the detectivity can be calculated through Equation (4):

$$D^* = \frac{R}{\sqrt{2eJ_d}}, \tag{4}$$

where $J_d$ is the dark current density.

4.3 *Experimental results and discussions*

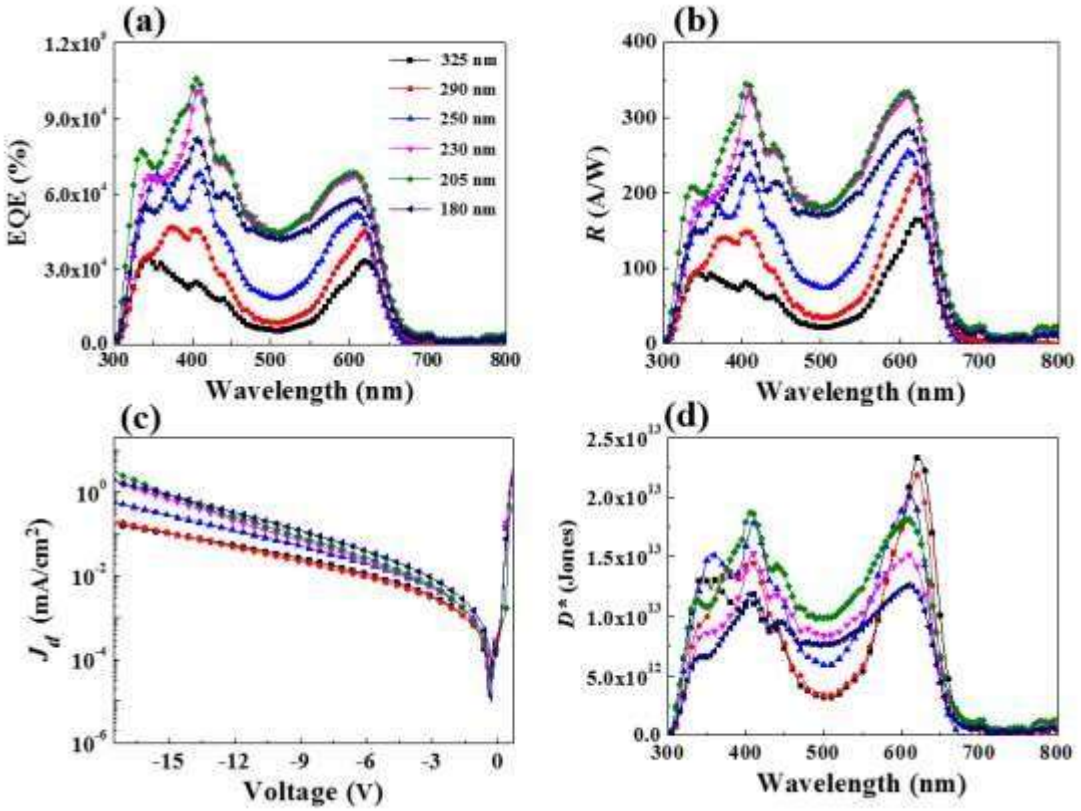


Fig. 4. Characteristics of OPD devices when $L$ is tuned. (a) The external quantum efficiency (EQE) spectra, (b) the

photoresponsivity ($R$) spectra, (c) the dark current density ($J_d$) versus the bias, and (d) the detectivity ($D^*$) spectra.

The electrical measurements for different OPDs indicate that the thickness of the active layer indeed has significant influences on the performances of the trap assisted PM effects. Figs. 4(a) and 4(b) show the EQE and $R$ spectra, respectively, of different OPDs measured at −17 V bias. It is seen clearly that the EQE and $R$ measured for the OPDs, made with two different active layer thicknesses of 325 nm and 290 nm, are the smallest over all curves although their absorption abilities are quite strong as indicated by Fig. 2(a) as well as by the measured absorption spectra of the whole device (not shown). With the decrease of the active layer, the EQE and $R$ are reduced; and the OPDs with a 205 nm thick active layer possess a maximum EQE of 105569% and a champion $R$ of 344 A/W at 405 nm wavelength, corresponding to an enhancement of 330% as compared to those when $L$ = 325 nm (EQE = 24875%, $R$ = 80 A/W). An obvious demerit of thinning the active layer is the worsening of the dark current ($J_d$) as shown in Fig. 4(c), which is due to the lowering of the series resistance. Ascribed to the trade off of EQE and $J_d$, the detectivity $D^*$ spectra of the OPDs have different performances at different wavelength ranges, as shown in Fig. 4(d). It is found that at wavelength range shorter than 500 nm, $D^*$ reaches the highest of $1.87\times10^{13}$ Jones with $L$ = 205 nm, while at wavelength range longer than 500 nm, the highest $D^*$ is $2.32\times10^{13}$ Jones with $L$ = 325 nm.

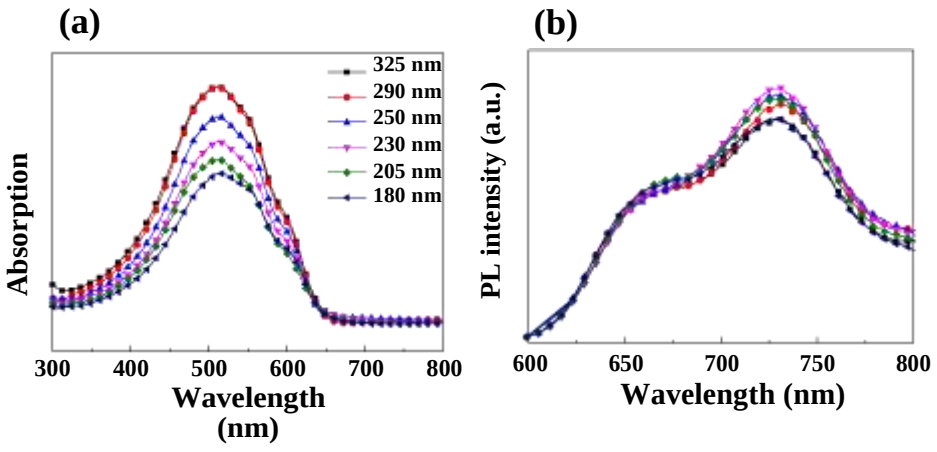


Fig. 5. (a) Absorption and (b) PL spectra of the multilayer ITO/PEDOT:PSS/ P3HT:$PC_{70}BM$ made with different

active layer thicknesses.

The performances of EQE are explained according to the equation (2) of EQE. Here, on the assumption that $\tau$ is constant for different OPDs, both $\chi$ and $L$ can affect the EQE of OPDs. On one hand, the decrease of $L$ directly brings forward the decrease of $T$, causing an enhancement on EQE. On the other hand, the decrease of $L$ from 325 nm to 180 nm also increase the absorption of light near the Al electrode as indicated in Fig. 2(c), which should lead to a greater $\chi$ and thus an enhancement on EQE as well. However, as we observed, the EQE and photoresponsivity are optimized at $L$ = 205 nm instead of the smallest $L$. To explain the observation, we further fabricated the multilayer films of ITO/PEDOT:PSS/P3HT:$PC_{70}$BM with varied active layer thicknesses and measured their absorption spectra and PL spectra, as displayed in Figs. 5(a) and 5(b), respectively. One sees from Fig. 5(a) that the absorption efficiencies over the broad wavelength range from 300 nm to 650 nm increase gradually with the increase of the thickness of the active layer from 180 nm to 290 nm. And the two absorption curves of $L$ = 290 nm and 325 nm are more or less the same. The study of absorption spectra indicates that the P3HT:$PC_{70}$BM layer with a larger $L$ has a higher exciton generation rate, therefore a higher PL intensity would be expected if the exciton generation rates are the same for different films. However, it is interesting to find out from Fig. 5(b) that the PL intensity at the emission peak of ~730 nm is optimized when $L$ = 230 nm, reflecting that the film has a higher exciton dissociation rate which limits the radiative transition of excitons. We then measured the surface morphologies of the P3HT:$PC_{70}$BM films and the results are shown in Fig .6. It is seen that, with the decrease of $L$ from 325 nm to 180 nm, the surface roughness (RMS) of the active layer first decreases and then increases. The corresponding RMS in Figs. 6(a)-6(f) are 3.47 nm, 2.59 nm, 2.10 nm, 1.44 nm, 2.11 nm, and 2.66 nm, respectively. The smallest RMS is obtained when $L$ = 230 nm, of which the PL intensity is also the highest as shown

in Fig. 5(b). This reflects that the enhanced exciton dissociation rate at $L$ = 230 nm is due to the smoother film morphology. In combination with the exciton generation and exciton dissociation properties, the amount of photogenerated tapped electrons near the Al electrode (which relates to $\chi$ in the equation of EQE) get optimized at $L$ greater than 180 nm. Therefore, although the decrease of $L$

induces a smaller $T$ and thus a greater EQE, the champion EQE values were achieved at $L$ = 205 nm.

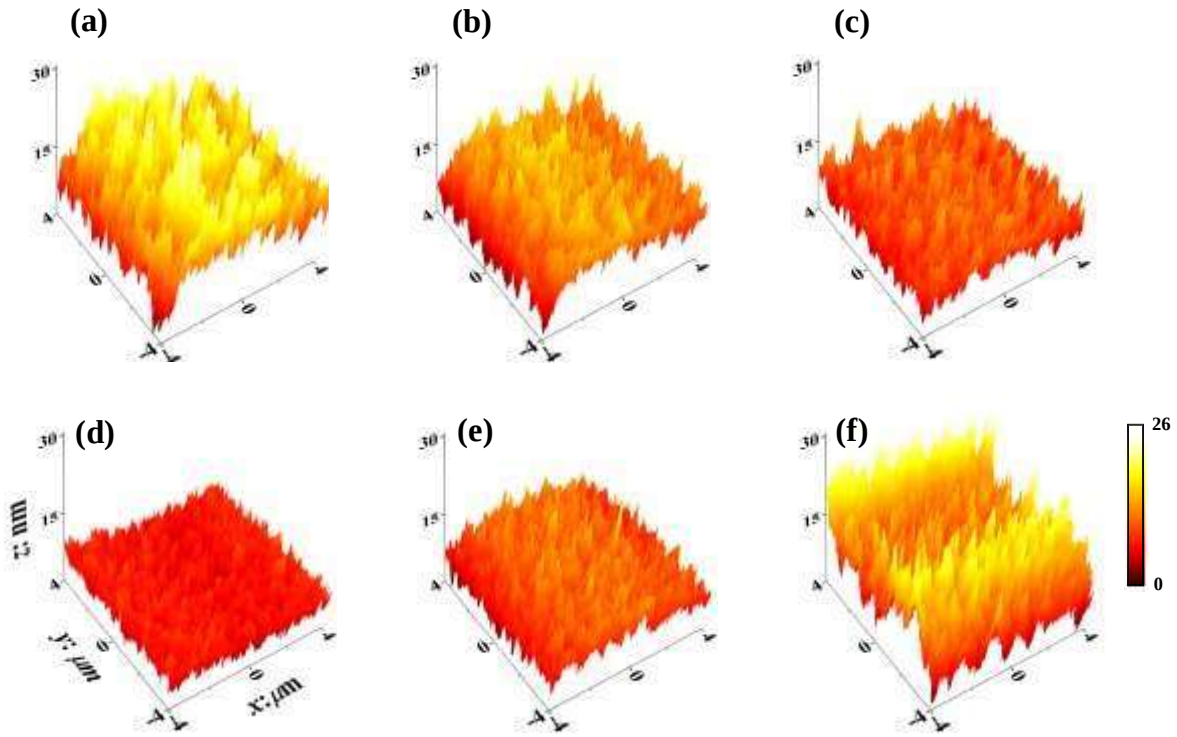


Fig. 6. AFM images measured for the ITO/PEDOT:PSS/ P3HT:$PC_{70}$BM films with different P3HT:$PC_{70}$BM layer thicknesses of (a) 325 nm, (b) 290 nm, (c) 250 nm, (d) 230 nm, (e) 205 nm, and (f) 180 nm.

## 5. Conclusions

The performance of the PMtype OPDs with a P3HT:$PC_{70}$BM (100:1) active layer was studied systematically by tuning the active layer thickness. In theoretical calculation, the change of the active

layer thickness shows vital influences on the distribution of light absorption, i.e., the distribution of exciton generation in the active layer. It shows that the thinner the active layer, the stronger exciton

generation near the Al electrode. In the following experiment studies, it has been confirmed that the EQE spectral and the dark current of OPDs strongly depend on the thickness of the active layer. It is demonstrated that the highest EQE (105569%) was achieved at 405 nm wavelength under -17 V bias when the thickness of active layer is 205 nm. Through the absorption, photoluminescence, and surface morphology studies of the ITO/PEDOT:PSS/P3HT:$PC_{70}BM$(100:1) multilayer films, we have found that the active layer thickness also affects the exciton dissociation rate and the film with a 230 nm thick active layer possesses the highest exciton dissociation rate due to improved morphologies. Therefore, although the thinnest active layer has the strongest exciton generation near the Al electrode according to the simulation results, the amount of photogenerated electrons at that region is not optimal. It is the amount of the photogenerated electrons and the hole transport time through the active layer, both of which are influenced by the active layer thickness, codetermines the gain intensity, resulting in the champion EQE achieved when a 205 nm thick active layer is applied. In addition, because the lowest dark current was realized when the active layer of 325 nm thick is used, the corresponding detectivity reaches the highest of $2.32\times10^{13}$ Jones at wavelength range longer than 500 nm. But at wavelength range shorter than 500 nm, $D^*$ reaches the highest of $1.87\times10^{13}$ Jones with the 205 nm thick active layer. It is believed that the findings in this work can also be applied in other PM type OPDs. Our work is helpful for the development of low cost high performance organic photodetectors.

**Acknowledgements**

We are grateful for support from the National Natural Science Foundation of China (61775156, 61805172, 61571317, and U1710115), the Natural Science Foundation of Shanxi Province (201701D211002), Henry Fok Education Foundation Young Teachers fund, Young Sanjin Scholars

Program, Key Research and Development (International Cooperation) Program of Shanxi Province (201603D421042), and Platform and Base Special Project of Shanxi Province (201605D131038). We also thank Fujun Zhang, Wenbin Wang, and Jianli Miao at Beijing Jiaotong University for their guidance on the part of experimental details.

## References

[1] D. Baierl, B. Fabel, P. Gabos, L. Pancheri, P. Lugli, and G. Scarpa, Solution-processable inverted organic photodetectors using oxygen plasma treatment. Org. Electron, **11**(7) (2010) 1199-1206.

[2] K. S. Nalwa, Y. Cai, A. L. Thoeming, J. Shinar, R. Shinar, and S. Chaudhary, Polythiophene-fullerene based photodetectors: tuning of spectral response and application in photoluminescence based (bio)chemical sensors. Adv. Mater, **22**(37) (2010) 4157-61.

[3] D.-S. Leem, K.-H. Lee, K.-B. Park, S.-J. Lim, K.-S. Kim, Y. Wan Jin, and S. Lee, Low dark current small molecule organic photodetectors with selective response to green light. Appl. Phys. Lett, **103**(4) (2013) 043305.

[4] N. Li, Y. S. Lau, Z. Xiao, L. M. Ding and F.R. Zhu, NIR to visible light upconversion devices comprising an NIR charge generation layer and a perovskite emitter, Adv. Opt. Mater., 2018, doi: 10.1002/adom.201801084..

[5] T. Wang, Y. Hu, Z. Deng, Y. Wang, L. Lv, L. Zhu, Z. Lou, Y. Hou, and F. Teng, High sensitivity, fast response and low operating voltage organic photodetectors by incorporating a water/alcohol soluble conjugated polymer anode buffer layer. RSC. Adv, **7**(3) (2017) 1743-1748.

[6] F. Guo, B. Yang, Y. Yuan, Z. Xiao, Q. Dong, Y. Bi, and J. Huang, A nanocomposite ultraviolet photodetector based on interfacial trap-controlled charge injection. Nat. Nanotechnol, **7**(12) (2012) 798-802.

[7] X. Li, S. Wang, Y. Xiao, and X. Li, A trap-assisted ultrasensitive near-infrared organic photomultiple photodetector based on Y-type titanylphthalocyanine nanoparticles. J. Mater. Chem. C, **4**(24) (2016) 5584-5592.

[8] L. Li, F. Zhang, W. Wang, Q. An, J. Wang, Q. Sun, and M. Zhang, Trap-assisted photomultiplication polymer photodetectors obtaining an external quantum efficiency of 37,500%. ACS. Appl. Mater. Interfaces, **7**(10) (2015) 5890-7.

[9] L. Li, F. Zhang, W. Wang, Y. Fang, and J. Huang, Revealing the working mechanism of polymer photodetectors with ultra-high external quantum efficiency. Phys. Chem. Chem. Phys, **17**(45) (2015) 30712-20.

[10] H. Wei , Y. Fang , Y. Yuan , L. Shen , and J. Huang, Trap Engineering of CdTe Nanoparticle for High Gain, Fast

Response, and Low Noise P3HT:CdTe Nanocomposite Photodetectors. Adv. Mater., **27** (2015) 4975-4981.

[11] W. Wang, F. Zhang, M. Du, L. Li, M. Zhang, K. Wang, Y. Wang, B. Hu, Y. Fang, and J. Huang, Highly

Narrowband Photomultiplication Type Organic Photodetectors. Nano. Lett, **17**(3) (2017) 1995-2002.

[12] L. Shi, Q. Liang, W. Wang, Y. Zhang, G. Li, T. Ji, Y. Hao, and Y. Cui, Research Progress in Organic

Photomultiplication Photodetectors. Nanomaterials (Basel), **8**(9) (2018).

[13]G. Konstantatos and E. H. Sargent, Nanostructured materials for photon detection. Nat. Nanotechnol, **5**(6) (2010)

391-400.

[14] X. Wang, Z. Cheng, K. Xu, H. K. Tsang, and J.-B. Xu, High-responsivity graphene/silicon-heterostructure waveguide photodetectors. Nat. Photonics, **7**(11) (2013) 888-891.

[15] F. H. Koppens, T. Mueller, P. Avouris, A. C. Ferrari, M. S. Vitiello, and M. Polini, Photodetectors based on graphene, other two-dimensional materials and hybrid systems. Nat. Nanotechnol, **9**(10) (2014) 780-93.

[16] S.-h. Wu, W.-l. Li, B. Chu, Z.-s. Su, F. Zhang, and C. S. Lee, High performance small molecule photodetector with broad spectral response range from 200 to 900 nm. Appl. Phys. Lett, **99**(2) (2011) 023305.

[17] S. F. Alvarado, P. F. Seidler, D. G. Lidzey, and D. D. C. Bradley, Direct Determination of the Exciton Binding Energy of Conjugated Polymers Using a Scanning Tunneling Microscope. Phys. Rev. Lett, **81**(5) (1998) 1082-1085.

[18] G. Caserta, B. Rispoli, and A. Serra, Space-Charge-Limited Current and Band Structure in Amorphous Organic Films. Phys. Status Solidi, **35**(1) (1969) 237-248.

[19] M. Hiramoto, K. Nakayama, I. Sato, H. Kumaoka, and M. Yokoyama, Photocurrent multiplication phenomena at organic/metal and organic/organic interfaces. Thin Solid Films, **331**(1-2) (1998) 71-75.

[20] M. Hiramoto, A. Miki, M. Yoshida, and M. Yokoyama, Photocurrent multiplication in organic single crystals. Appl. Phys. Lett, **81**(8) (2002) 1500-1502.

[21] Y. Fang, F. Guo, Z. Xiao, and J. Huang, Large Gain, Low Noise Nanocomposite Ultraviolet Photodetectors with a Linear Dynamic Range of 120 dB. Adv. Opt. Mater **2**(4) (2014) 348-353.

[22] T. K. Däubler, D. Neher, H. Rost, and H. H. Hörhold, Efficient bulk photogeneration of charge carriers and photoconductivity gain in arylamino-PPV polymer sandwich cells. Phys. Rev. B: Condens. Matter **59**(3) (1999)

1964-1972.

[23] I. H. Campbell and B. K. Crone, Bulk photoconductive gain in poly(phenylene vinylene) based diodes. J. Appl. Phys, **101**(2) (2007) 024502.

[24] W. Wang, F. Zhang, L. Li, M. Gao, and B. Hu, Improved Performance of Photomultiplication Polymer

Photodetectors by Adjustment of P3HT Molecular Arrangement. ACS. Appl. Mater. Interfaces, **7**(40) (2015) 22660-8.

[25] R. Dong, C. Bi, Q. Dong, F. Guo, Y. Yuan, Y. Fang, Z. Xiao, and J. Huang, An Ultraviolet-to-NIR Broad Spectral

Nanocomposite Photodetector with Gain. Adv. Opt. Mater, **2**(6) (2014) 549-554.

[26] D.Liu, Q. Liang, G. Li, X. Gao,W. Wang, Q. Zhan, T. Ji, Y. Hao, and Y. Cui, Improved Efficiency of Organic Photovoltaic Cells by Incorporation of AuAg-Alloyed Nanoprisms. IEEE J. PHOTOVOLT., **7**(4) (2017) 1036-1041.

[27] Y. Cui, H. Zhao, F. Yang, P. Tong, Y. Hao, Q. Sun, F. Shi, Q. Zhan, H. Wang and F. R. Zhu, Efficiency enhancement in organic solar cells by incorporating silica-coated gold nanorods at the buffer/active interface. J. Mater. Chem. C, **3** (2015) 9859.

[28] W. Wang, F. Zhang, L. Li, M. Zhang, Q. An, J. Wang, and Q. Sun, Highly sensitive polymer photodetectors with a broad spectral response range from UV light to the near infrared region. J. Mater. Chem. C, **3**(28) (2015) 7386-7393.

[29] M. Gao, W. Wenbin, L. Li, J. Miao, and F. Zhang, Highly sensitive polymer photodetectors with a wide spectral response range. Chin. Phys. B, **26**(1) (2017) 530-536.

[30] M. R. Esopi, M. Calcagno, and Q. Yu, Organic Ultraviolet Photodetectors Exhibiting Photomultiplication, Low Dark Current, and High Stability. Adv. Mater. Technol, (2017) 1700025.

[31] L. Li, F. Zhang, J. Wang, Q. An, Q. Sun, W. Wang, J. Zhang, and F. Teng, Achieving EQE of 16,700% in P3HT:$PC_{71}BM$ based photodetectors by trap-assisted photomultiplication. Sci. Rep, **5**(1) (2015).

[32] W. Wang, F. Zhang, H. Bai, L. Li, M. Gao, M. Zhang, and X. Zhan, Photomultiplication photodetectors with P3HT:fullerene-free material as the active layers exhibiting a broad response. Nanoscale, **8**(10) (2016) 5578-86. [33] W. Wang, Y. Cui, K. H. Fung, Y. Zhang, T. Ji, and Y. Hao, Comparison of Nanohole-Type and Nanopillar-Type

Patterned Metallic Electrodes Incorporated in Organic Solar Cells. Nanoscale Res. Lett, **12**(1) (2017) 538.

[34] W. Wang, Y. Cui, K. H. Fung, Y. Zhang, T. Ji, and Y. Hao, Comparison of Nanohole-Type and Nanopillar-Type

Patterned Metallic Electrodes Incorporated in Organic Solar Cells. Nanoscale Res. Lett., **12**(1) (2017).

[35] Z. Wang, Y. Hao, W. Wang, Y. Cui, Q. Sun, T. Ji, Z. Li, H. Wang, and F. R. Zhu, Incorporating silver-$SiO_2$ core-shell nanocubes for simultaneous broadband absorption and charge collection enhancements in organic solar cells. Synthetic Met., **220** (2016) 612-620.

[36] W. Wang, Y. Hao, Y. Cui, X. Tian, Y. Zhang, H. Wang, F. Shi, B. Wei, and W. Huang, High-efficiency, broad-band and wide-angle optical absorption in ultra-thin organic photovoltaic devices. Opt. Express, **22** (2014)

A376-85.